ALMA Observations of the Galactic Center: SiO Outflows and High Mass Star Formation near Sgr A*

F. Yusef-Zadeh[1], M. Royster[1], M. Wardle[2], R. Arendt[3], H. Bushouse[4], S. Gillessen[5], D. Lis[6], M. W. Pound[7], D. A. Roberts[1], B. Whitney[8] and A. Wooten[9]

[1]*Department of Physics and Astronomy, Northwestern University, Evanston, IL 60208*

[2]*Department of Physics and Astronomy, Macquarie University, Sydney NSW 2109, Australia*

[3]*CREST/UMBC/NASA GSFC, Code 665, Greenbelt, MD 20771*

[4]*Space Telescope Science Institute, 3700 San Martin Drive, Baltimore, MD 21218*

[5]*Max Planck Institut für Extraterrestrische Physik, Postfach 1312, D-85741 Garching, Germany*

[6]*California Institute of Technology, MC 320-47, Pasadena, CA 91125*

[7]*University of Maryland, Department of Astronomy, MD 20742*

[8]*Space Science Institute, 4750 Walnut Street, Suite 205, Boulder, CO 80301*

[9]*National Radio Astronomy Observatory, Charlottesville, VA 22903*

ABSTRACT

Using ALMA observations of the Galactic center with a spatial resolution of $2.61'' \times 0.97''$, we detected 11 SiO (5-4) clumps of molecular gas in the within 0.6pc ($15''$) of Sgr A*, interior of the 2-pc cicumnuclear molecular ring. Three SiO (5-4) clumps closest to Sgr A* show the largest central velocities of ~ 150 km s^{-1} and broadest asymmetric linewidths with total linewidths FWZI $\sim 110 - 147$ km s^{-1}. Other clumps are distributed mainly to the NE of the ionized mini-spiral with narrow linewidths of FWHM $\sim 11 - 27$ km s^{-1}. Using CARMA data, LVG modeling of the broad velocity clumps, the SiO (5-4) and (2-1) line ratios constrain the column density N(SiO) $\sim 10^{14}$ cm^{-2}, and the H_2 gas density $n_{H_2} = (3-9) \times 10^5$ cm^{-3} for an assumed kinetic temperature 100-200K. The SiO

(5-4) clumps with broad and narrow linewidths are interpreted as highly embedded protostellar outflows, signifying an early stage of massive star formation near Sgr A* in the last 10^4 years. Additional support for the presence of YSO outflows is that the luminosities and velocity widths lie in the range detected from protostellar outflows in star forming regions in the Galaxy. Furthermore, SED modeling of stellar sources along the N arm show two YSO candidates near SiO clumps supporting in-situ star formation near Sgr A*. We discuss the nature of star formation where the gravitational potential of the black hole dominates. In particular, we suggest that external radiative pressure exerted on self-shielded molecular clouds enhance the gas density, before the gas cloud become gravitationally unstable near Sgr A*.

Subject headings: Galaxy: center - clouds - ISM: general - ISM - radio continuum - stars: formation

1. Introduction

There is compelling evidence that the compact radio source Sgr A* is located at the very dynamical center of our galaxy and coincides with a $4 \times 10^6 M_\odot$ black hole (Ghez *et al.* 2008; Gillessen *et al.* 2009). Given the strong tidal shear of the back hole, in-situ star formation is forbidden unless the gas density is large enough for self-gravity to become important. *In-situ* star formation near Sgr A* is considered as a viable mechanism in which cloud capture by the black hole forms a massive and dense gaseous disk around the black hole. The disk becomes unstable gravitationally, thus forming a new generation of stars (e.g., Levin and Beloborodov 2003; Nayakshin *et al.* 2007; Paumard *et al.* 2006; Lu *et al.* 2009; Mapelli *et al.* 2012; Wardle & Yusef-Zadeh 2008; Bonnell & Rice 2008; Alig *et al.* 2012). This formation scenario has been applied to the young population of stars distributed in a stellar disk on a scale of 0.03-0.3 pc, to the 2-5pc circumnuclear ring of molecular gas (CND or CNR) orbiting Sgr A* as well as to AGNs with megamaser disks (Wardle and Yusef-Zadeh 2008; 2012). The Galactic center provides an opportunity for testing models of stellar birth with far reaching implications on the nature of star formation in the nuclei of galaxies hosting massive black holes.

Because the age of the stellar cluster orbiting Sgr A* is several million years old, it is not possible to identify signatures of early phases of star formation activity near the black hole. However, a number of recent studies suggest infrared excess sources in the N arm as well as young stellar object (YSO) candidates in IRS 13N within a projected distance of 0.12 pc ($3''$) from Sgr A* (e.g., Viehmann *et al.* 2006; Eckart *et al.* 2012; Nishiyama and Schödel 2013).

These measurements imply that star formation is taking place on a time scale of $\sim 10^5$ years. On a larger scale of $50'' - 100''$ or projected distance of 2-4 pc (assuming that the Galactic center distance is 8.5 kpc), the molecular ring (Jackson *et al.* 1993; Montero-Castano *et al.* 2009, Martin *et al.* 2012) that encircles Sgr A* with a rotational velocity of ~ 100 km s^{-1} has shown signatures of massive star formation activity on a time scale of $\sim 10^4$ years (Yusef-Zadeh *et al.* 2008).

Here, we present the earliest signatures of on-going star formation on a size scale of about $11''$ (0.44 pc) from Sgr A* evidenced by the presence of SiO (5-4) line emission from the interior of the molecular ring. The SiO molecule is an *excellent* tracer of protostellar outflows and is shock excited where silicon is removed from dust grains, significantly increasing gas-phase abundance (Martin-Pintado, *et al.* 1992; Gibb *et al.* 2007). Given that the excitation of the SiO (5-4) line emission requires high density and excitation temperature, the Galactic center with its warm and dense ISM is a natural place for probing highly excited SiO (5-4) line emission.

2. Observations and Data Reduction

ALMA: The data were obtained through the ALMA Science Verification process on June 26, 2011. Utilizing only twelve of the 12 m antennas, the observations consisted of a 7-point mosaic at the position of Sgr A*: $(\alpha, \delta) = 17^h45^m40^s.04, -29°0'28''.12$. Titan was initially used as the flux calibrator and 3C279 as the initial bandpass and phase calibrators. NRAO 530 was observed periodically to correct for any changes in phase and amplitude as function of time. Four basebands of 1.875 GHz were used with the high spectral resolution which contained 3840 channels each. The spectral windows were centered at roughly: 216.2 GHz, 218.0 GHz, 231.9 GHz, and 233.7 GHz. The RRL is found in the third window at 231.9 GHz. The SiO (5-4) line emission is centered at 217.105 GHz. The editing and calibration of the data was carried out by the Science Verification team in CASA. The imaging was completed by modifying the supplied imaging script. SiO 5-4 fell at the intersection of the first two basebands at 216.2 GHz and 218.0 GHZ. As a result, care was taken to note any changes in amplitude and phase at the edge channels in combining the two windows. A linear continuum was fitted and subtracted from the line-free channels before CLEANing. After all averaging, the final data cube has a spectral resolution of 6.74 km s^{-1} (1.220 MHz) and a total velocity range of 1000 km/s. We studied velocity structures within 440 km s^{-1} with the spatial resolutions of $2.61'' \times 0.97''$. Assuming that the SiO (5-4) brightness temperature is twice its minimum value, the beam filling factor is 0.5, thus, 1 mJy is equivalent to $T_{MB} = 20.5$ mK.

CARMA: The SiO (2-1) line data were taken with the Combined Array for Research in Millimeter-wave Astronomy (CARMA) during the 2009 and 2010 observing seasons in the D and C array configurations. The array consisted of six 10.4m antennas and nine 6.1m antennas and the maps were made on a 127-point hexagonal mosaic, Nyquist-sampling the 10.4m antenna primary beam. The spatial resolution and spectral resolutions of the final maps are $8.87'' \times 4.56''$ and 6.74 km s^{-1}, respectively. Using the beam filling factor of 0.5, 1 mJy is equivalent to $T_{MB} = 7.96$ mK.

3. Results and Discussion

Figure 1a shows a composite 3.6cm continuum image of the three arms of the mini-spiral (Sgr A West) surrounded by the molecular ring as traced by HCN line emission (Christopher *et al.* 2005). The inner $1'$ (2.4pc) of the molecular ring, as observed with ALMA, shows a large concentration of molecular clumps in the SiO (5-4) line emission. The distribution of molecular and ionized gas orbiting Sgr A* is generally considered in terms of a central cavity that consists of ionized gas of Sgr A West coupled to the surrounding molecular ring (e.g. Roberts and Goss 1993; Serabyn and Lacy 1985). In particular, the coincidence in the geometry and kinematics of the western edge of the molecular ring (Western Arc) and the ionized gas suggests a picture in which the western half of the molecular ring and Sgr A West are dynamically coupled to each other (e.g. Güsten *et al.* 1987; Montero-Castano *et al.* 2009). The SiO (5-4) line emission is clumpy and its distribution in the western edge of the molecular ring is consistent with this picture. The nature of the association between the N and E arms of ionized gas and the molecular ring, however, it is not clear.

A string of SiO clumps is found in the region between the N and E arms of Sgr A West. A close up view of these clumps is shown in Figure 1b where the distribution of SiO (5-4) line emission superimposed on a 3.6cm continuum image. What is most interesting is the presence of SiO clumps in the interior of the ring which is expected to be dominated by the central cavity of ionized gas and [OI] gas, devoid of any molecular gas. If the high density molecular gas interior to the ring is massive enough, it has important consequence in perturbing the dynamics of stars close to Sgr A*. Figure 1b also shows two clumps (green), with velocities $v_r \sim 136$ to 160 km s^{-1}, and FWHM linewidths 47 to 55 km s^{-1}. These ALMA clumps, 1 and 11, are located about $7''$ NE and $11''$ SW of Sgr A*, respectively, and do not follow the kinematics of the molecular ring orbiting Sgr A*. Figure 1c shows the positions of these highly redshifted velocity clumps on a 3.6μm image taken with the VLT. Clumps 1 and 2 lie $\sim 2''$ west of IRS 1W which is known to be a hot, mass-losing W-R star with a bow shock structure (Tanner *et al.* 2003).

To illustrate the kinematics of SiO (5-4) molecular clumps, Figure 2 shows the distribution of SiO (5-4) peak line emission and the spectra of 11 clumps within the ring. There may be diffuse SiO material between clumps but our interferometric data are not sensitive to detect it. The kinematics of SiO (5-4) line emission and absorption from the the molecular ring and its interior will be given elsewhere. Columns 1 to 7 of Table 1 list the source numbers, the coordinates, the intensity of the peak emission, Gaussian fitted central velocity and FWHM linewidths and full width at zero intensity (FWZI) of 11 sources labeled on Figure 2. FWZI linewidths are presented because many sources show velocity profiles with blue-shifted wings (e.g., clumps 1, 2, 11). Clumps 4 to 8 run parallel to the eastern edge of the N arm of ionized gas showing typical linewidths between 11 and 21 km $s^{-1}$and peak radial velocities that decrease from 37.8 km s^{-1} at Clump 8 to 7.4 km s^{-1}at Clump 4. The trend in radial velocity change in molecular clumps is consistent with the trend noted in the kinematics of ionized gas of the N arm. However, the central velocities of ionized and atomic [OI] gas of the N arm are ∼100 km s^{-1} and decrease to 0 km s^{-1} as the ionized gas approaches closer to Sgr A* (e.g., Roberts and Goss 1993; Jackson *et al.* 1993; Zhao *et al.* 2011). The kinematics of SiO (5-4) are dissimilar to those of the ionized gas of the N arm and the "tongue" of neutral [OI] gas. The spatial and velocity distributions of SiO (5-4) suggest a clumpy and dense molecular cloud which appears to lie in the interior of the molecular ring.

Clumps 1, 2 and 3 defy the kinematical trend of the N arm. These sources with their highly red-shifted (<160 km s^{-1}) and blue-shifted velocity (-28 km s^{-1}) components lie adjacent to the ionized gas of the N arm, with dissimilar velocities. Figure 3a shows contours of highly red-shifted SiO (5-4) line emission from Clumps 1 and 2 superimposed on a 3cm continuum image of the N arm. The SiO line emission from Clump 1 appears to be elongated to the NE with non-Gaussian velocity profiles having blue-shifted wings. Another morphological structure of the N arm is the wavy structure along the direction of the flow (Yusef-Zadeh and Wardle 1993; Zhao *et al.* 2012). Figure 3b shows contours of SiO (5-4) emission from Clump 5 and are superimposed on a 3cm continuum image. We note that Clump 3 lies adjacent to the wavy structure. The spectrum of this clump shows non-circular velocity peaking at v∼ −28 km s^{-1} and linewidth of $v_{\rm FWHM} \sim 27$ km s^{-1} with a broad blue-shifted wing extending to −100 km s^{-1}. This radial velocity is inconsistent with circular motion orbiting Sgr A*. We note several radio dark clouds (Yusef-Zadeh 2012) to the east of the N arm in Figures 3a,b where Clumps 1, 2 and 3 lie. These dark features trace molecular gas and are embedded in the ionized gas of the N arm. Although the morphology of ionized gas at the location of Clumps 1 and 3 suggests that the flow of ionized gas is distorted as a result of its interactions with molecular clumps, the kinematics of the molecular and ionized gas are inconsistent with the interaction picture. Future observations will be able to determine if

these outflow sources are dynamically interacting and bending the flow of ionized gas in the N arm.

Protostellar Outflows: To examine the physical properties of SiO clumps, we focus on SiO (5-4) and (2-1) line profiles, as shown in Figure 3c, with peak line emission $T_{MB} \sim 0.95$ and 0.65 K, for Clump 1 and $T_{MB} \sim 1.1$ and 1 K, for Clump 11 at center velocity of ~ 147 and ~ 136 km s^{-1}, respectively. The similarity of SiO (5-4) and (2-1) line profiles toward Clumps 1 and 11 is a classic signature of one-sided molecular outflows in star forming regions (e.g., Plambeck & Menten 1990). We applied the Large Velocity Gradient (LVG) model in order to derive constraints on molecular gas, density and column density of SiO line emission. The result of this analysis is shown in Figure 3d with a plot of molecular gas density as a function of temperature for Clumps 1 and 11. The application of the LVG excitation code to Clumps 1 and 11 constrains the gas density of hydrogen nuclei $n_{H_2} \sim (3-9) \times 10^5$ cm^{-3} within a temperature range 100-200K. Multi-transition CO and NH_3 studies of the inner 2pc of the Galactic center have derived kinetic temperature $(1-2) \times 10^2$K and warm gas in the interior of the molecular ring (Bradford *et al.* 2005; Herrnstein and Ho 2005). The column density of SiO per velocity width $N(SiO)/\Delta v \sim 1.7 - 2.4 \times 10^{12}$ cm^{-2} km s^{-1} is better constrained than the gas density, as shown in the bottom panel of Figure 3d. Using the equivalent widths of the two lines, the column densities of SiO for Clumps 1 and 11 are estimated to be $N(SiO) \sim 8.6 \times 10^{13}$ and $\sim 1.3 \times 10^{14}$ cm^{-2}, respectively. The total mass of molecular gas is estimated to be $\sim 0.2\ M_\odot$ using clump radius 0.03pc (0.79″) and $n_{H_2} = 10^6$ cm^{-3}. This corresponds to a column density of 1.8×10^{23} cm^{-2} and SiO abundance of 5.6×10^{-10}. Using the estimated size and the FWHM of the velocity widths, the velocity gradient is estimated to be 833 and 165 km s^{-1} pc^{-1} for clumps with broad (~ 50 km s^{-1}) and narrow (~ 10 km s^{-1}) linewidths respectively. These imply that the clumps can not be bound by self-gravity because the collapse time scale is 12-58 times longer than the dynamical time scales $t_{dyn} \sim (0.3-1.5) \times 10^3$ years, thus are likely to be outflows from YSOs. The presence of blue-shifted velocity wings with non-circular radial velocities is also consistent with SiO outflows in which the approaching side of the outflow has burst through the edge of the molecular cloud.

One strong piece of evidence that the SiO sources are YSO outflows is that the luminosities and velocity widths lie in the range detected from protostellar outflows in star forming regions. Figure 4 shows a plot the SiO (5-4) luminosity versus full width at zero intensity for the detected sources inside the molecular ring, as well as that for samples of low-mass and high-mass YSOs (Gibb *et al.* 2004 and 2007, respectively). All three samples show the same wide range of velocity widths, and the luminosities of SiO clumps interior to the molecular ring fall in between those of the low-mass and high-mass YSOs. This strongly suggests that we have detected SiO emission from outflows associated with intermediate and high-mass

YSOs in the ring.

What drives the source of outflow? Using the same technique that identified a population of YSO candidates toward the inner few hundred pc of the Galaxy (Yusef-Zadeh *et al.* 2009), we identified two new YSO candidates in the N arm near Clumps 1 and 3. Figure 3e shows contours of SiO (5-4) emission from Clumps 1 and 5 superimposed on ratio map of L (3.6μm) to K (1.6 μm) band images from VLT observations. The ratio map shows the dusty environment of the N arm. The crosses coincide with the positions of sources with the positional uncertainty of 1.18″ at 8μm (Ramirez *et al.* 2008). The SEDs of these sources are analyzed by comparing a set of SEDs enhanced by a large grid of YSO models (Whitney *et al.* 2003; Robitaille *et al.* 2007), as Figure 3f shows their fitted SEDs. The source 526311 is classified as Stage I YSO candidates whereas the red source 526817 is a YSO candidate but its classification is uncertain These YSO candidates have typical age of 10^5 years. By fitting the SEDs, we derive masses of 34.3 ± 5.9 and 19.4 ± 2.5 $M_\odot$, luminosities $1.8 \pm 0.7 \times 10^5$ and $4.4 \pm 1.5 \times 10^4$ $L_\odot$ and mass-loss rates $5.1 \pm 0.1 \times 10^{-4}$ and $2.5 \pm 0.1 \times 10^{-4}$ $M_\odot$ yr^{-1} for clumps 1 and 5, respectively. YSO candidate 526817 coincides with the brightest source IRS 10E (Viehmann *et al.* 2006) at the center of Clump 3 whereas the YSO candidate 526817 is unresolved component of multiple sources in IRS 1. The proximity of massive YSO candidates, SiO (5-4) Clumps near IRS 1 and IRS 10 clusters containing W-R stars, suggest that there is still on-going star formation near these stellar clusters. Similar distribution of massive YSOs, and W-R stars are found in the IRS 13 cluster (Fritz *et al.* 2012; Eckart *et al.* 2012).

Star Formation Mechanism: We have shown the presence of several SiO (5-4) clumps within a pc of Sgr A*. Their SiO (5-4) luminosities, non-Gaussian velocity profiles, characterized to be unbound by self-gravity and proximity to dark radio clouds tracing dense gas, all point to the suggestion that these clumps are tracing YSOs with protostellar outflows. Thus, observations presented here reveal earliest signs of massive star formation near Sgr A* on a time scale of $\sim 10^4$ years. Additional support for star formation on a time scales of $\sim 10^5$ to $\sim 10^6$ years come from SED fitted YSO candidates with infrared excesses as well as young stellar disks orbiting Sgr A*, respectively. These suggest that star formation is continuous in the Galactic center.

The mechanism in which star formation can take place in this tidally stressed environment is not well understood. The H_2 density at the Galactic center, $\sim 10^6 - 10^7 \mathrm{cm}^{-3}$, is well below that needed for self-gravity to overcome the tidal field of the central black hole, i.e. $3.9 \times 10^8 (\mathrm{r/1pc})^{-3}$ cm^{-3}. Star formation in this region must therefore be triggered by significant compression of the ambient gas in the ring. Tidal squeezing of an elongated cloud can compress the gas in two directions however, it is not clear, if the density can be

increased by two orders of magnitude as the cloud approached Sgr A*. Here we consider two possibilities: (i) compression by the intense UV radiation field in the Galactic center, and (ii) clump-clump collisions.

Hot stars in the central parsec produce an intense radiation field with an effective temperature $\sim 3 \times 10^4$K and a luminosity of order 10^7 $L_\odot$. The radiation pressure is capable of producing significant compression. Equating the radiation pressure to the thermal pressure of the compressed molecular gas, i.e. $L/(4\pi\, c\, D^2) = 1.2 n_{H_2} kT$, where D is the distance to the center of the hot star distribution, yields $n_{H_2} \sim 1.3{\times}10^8 (L/10^7 L_\odot)(D/0.1pc)^{-2}(T/100K)^{-1}$ cm^{-3}, comparable to the critical density. It is therefore possible for the pressure associated with irradiation by the UV field to compress a gas clump to the point of gravitational collapse. Note, however, that the clump must be exposed to the radiation field for about $5{\times}10^4$ years for the compression to work its way through the entire clump.

Clump-clump collisions are an alternative method for producing SiO emission, either through the destruction of dust grains in large scale shock waves associated with the collision, or via outflows from YSOs formed because the compression associated with the shock waves triggered star formation. This model, however has difficulty in producing the number of sources. Suppose a clump in the interior to the ring has radius r, clump-clump velocity dispersion v and volume filling factor f. Then the number of clumps per unit volume is $n_{cl} = f/(4/3\pi r^3)$, the cross section for almost head-on collisions is $\sigma \sim 2\pi r^2$, and the time scale for a given clump to collide with another is $1/(n_{cl}\sigma v)$. For an ensemble of N clumps, the number of collisions per unit time is 0.5 N $n_{cl}\sigma v \approx N\, f\, v/r$. The collisional interaction time is approximately 2r/v , so the number of collisions occurring at any given time is $(N\, f\, v\, /r) \times (2r/v) = 2f\, N$. For the interior of the molecular ring with a radius of 15″, N=11, f=0.005, and the total number of collisions at any given time is less than 0.1, thus unlikely to explain the observed number of clumps.

In conclusions, ALMA observations show that the interior of the cicumnuclear molecular ring is filled with cold, dense gas and is a site of on-going star formation. We suggest that the required high gas density is enhanced by the strong external radiation field from young massive stars compressing the gas, thus inducing star formation. Future observations will determine the total mass of molecular gas residing inside the ring and will allow estimating the efficiency of star formation within a pc of Sgr A*.

This paper makes use of the following ALMA data: ADS/JAO.ALMA#2011.0.00005.SVProject code. ALMA is a partnership of ESO (representing its member states), NSF (USA) and NINS (Japan), together with NRC (Canada) and NSC and ASIAA (Taiwan), in cooperation with the Republic of Chile. The Joint ALMA Observatory is operated by ESO, AUI/NRAO and

NAOJ.

REFERENCES

Alig, C., Burkert, A., Johansson, P. H. & Schartmann, M. 2012, MNRAS 412, 486

Bonnell, I. A., & Rice, W. K. M. 2008, Science, 321, 1060

Bradford, C. M., Stacey, G. J., Nikola, T., *et al.* 2005, ApJ, 623, 866

Christopher, M. H., Scoville, N. Z., Stolovy, S. R., Yun, M. S. 2005, ApJ, 622, 346

Eckart, A., Muzic, K., Yazici, S., Shahzamanian, B. et al. 2012, A&A (arXiv1208.1907)

Ghez, A. M., Salim, S., Weinberg, N. N. *et al.* 2008, ApJ, 689, 1044

Gibb, A. G., Davis, C. J. & Moore, T. J. T. 2007, MNRAS, 382, 1212

Gillessen, S., Eisenhauer, F., Trippe, S. *et al.* 2009, ApJ, 692, 1075

Herrnstein, R. M. & Ho, P. T. P. 2005, ApJ, 620, 287

Jackson, J. M., Geis, N., Genzel, R., Harris, A. I., Madden, S. *et al.* 1993, ApJ, 402, 173

Levin, Y. & Beloborodov, A. M. 2003, ApJ, 590, L33

Lu, J. R., Ghez, A. M., Hornstein, S. D. *et al.* 2009, ApJ, 690, 1463

Mapelli, M., Hayfield, T., Mayer, L. & Wadsley, J. 2012, ApJ, 749, 168

Martin, M. Martin-Pintado, J., Montero-Castano, M. *et al.* 2012, A&A, 539, 29

Martin-Pintado, J., Bachiller, R., & Fuente, A. 1992, A&A, 254, 315

Montero-Castano, M., Herrnstein, R. M. & Ho, Paul T. P. 2009, ApJ, 695, 1477

Paumard, T., Genzel, R., Martins, F. *et al.* 2006, ApJ, 643, 1011

Nayakshin, S., Cuadra, J. & Springel, V. 2007, MNRAS, 379, 21

[Nishiyama(2013)]nishiyama13 Nishiyama, S. & Schödel, R. 2013, A&A, 549, 16

Plambeck, R. L. & Menten, K. M. 1990, ApJ, 364, 555

Ramirez, S. V. and Arendt, R. G. and Sellgren, K. *et al.* 2008, ApJS, 175, 147

Roberts, D. A. & Goss, W. M. 1993, ApJS, 86, 133

Robitaille, T. P., Whitney, B. A., Indebetouw, R. *et al.* 2007, ApJS, 169, 328

Serabyn, E. & Lacy, J. H. 1985, ApJ, 293, 445

Tanner, A., Ghez, A. M., Morris, M. R. & Christou, J. C. 2005, ApJ, 624, 742

[Viehmann(2006)]viehmann06 Viehmann, T., Eckart, A., Schod̈el, *et al.* 2006, ApJ, 642, 861

Wardle, M., & Yusef-Zadeh, F. 2008, ApJ, 683, L37

Wardle, M., & Yusef-Zadeh, F. 2012, ApJ, 750, L38

Whitney, B. A. and Wood, K. and Bjorkman, J. E. & Wolff, M. J., 2003, ApJ, 591, 1049

Yusef-Zadeh, F. 2012, ApJ, 759, 8

Yusef-Zadeh, F., Braatz, J., Wardle, M., & Roberts, D. 2008, ApJL submitted

Yusef-Zadeh, F., Hewitt, J. W., Arendt, R. G., Whitney, B., Rieke, G. *et al.* 2009, ApJ, 702, 178

Yusef-Zadeh, F. & Wardle, M. 1993, ApJ, 405, 584

Zhao, J.-H., Blundell, R., Moran, J. *et al.* 2010, ApJ, 723, 1097

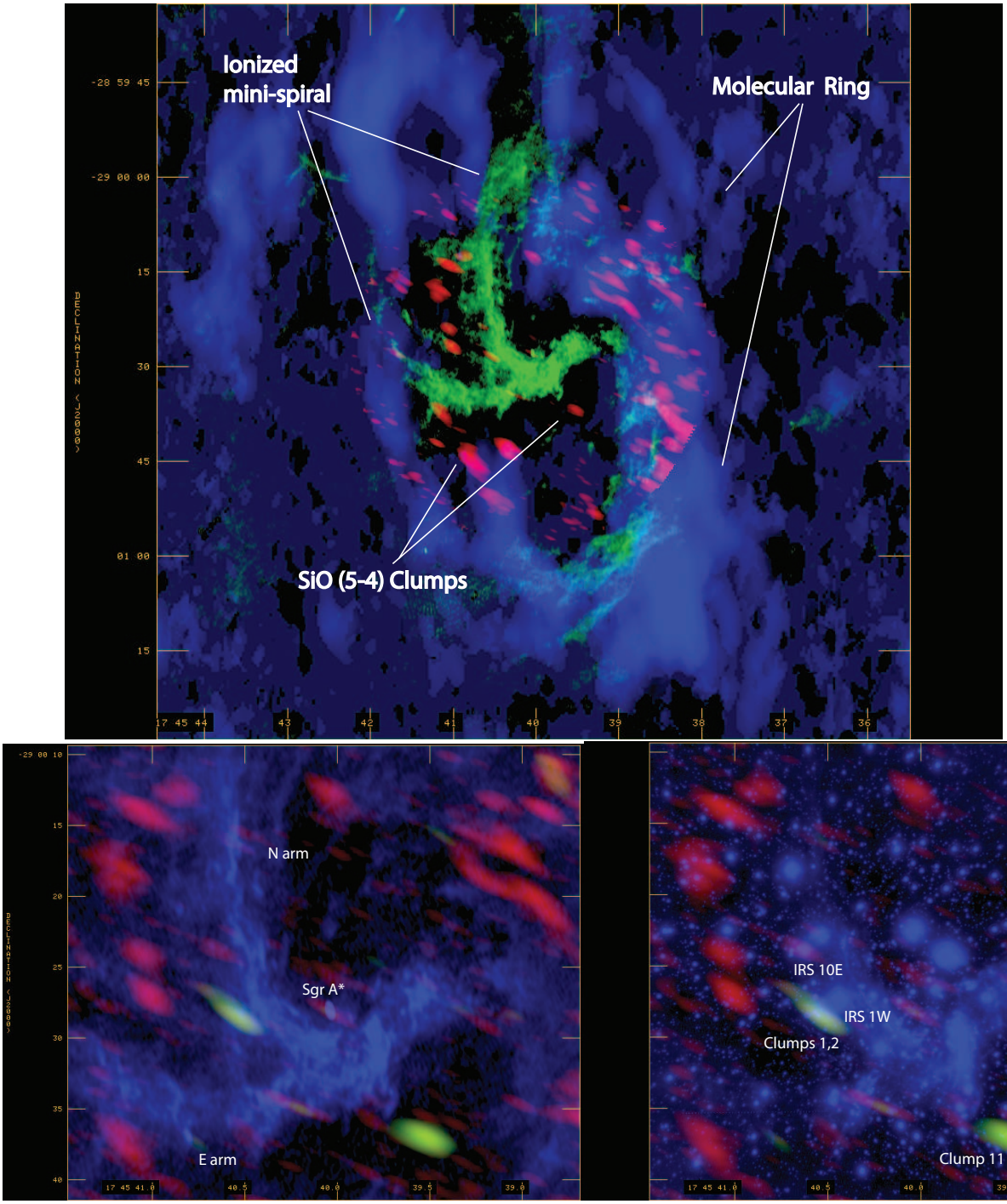

Fig. 1.— *(a) Top* A composite image of the inner 2′ of the Galactic center: 3.6cm continuum image of Sgr A West (green), HCN (1-0) emission from the molecular ring (blue; Christopher *et al.* 2005) and SiO (5-4) line emission from the central region of the ring (red) *(b) Bottom Left* The distribution of SiO line emission (red) integrated over velocities $150 < v < 200$ km s^{-1} and superimposed on a 3.6cm continuum image (blue). The edge of the SiO (5-4) clump distribution is noisier because of shorter integration time and is limited by the size of the region mapped by ALMA. The highest redshifted velocity SiO (5-4) clumps 1 and 11 are shown in green. *(c) Bottom Right* Similar to (a) except that a 3.6μm image taken with the VLT in blue replaces the 3.6cm image.

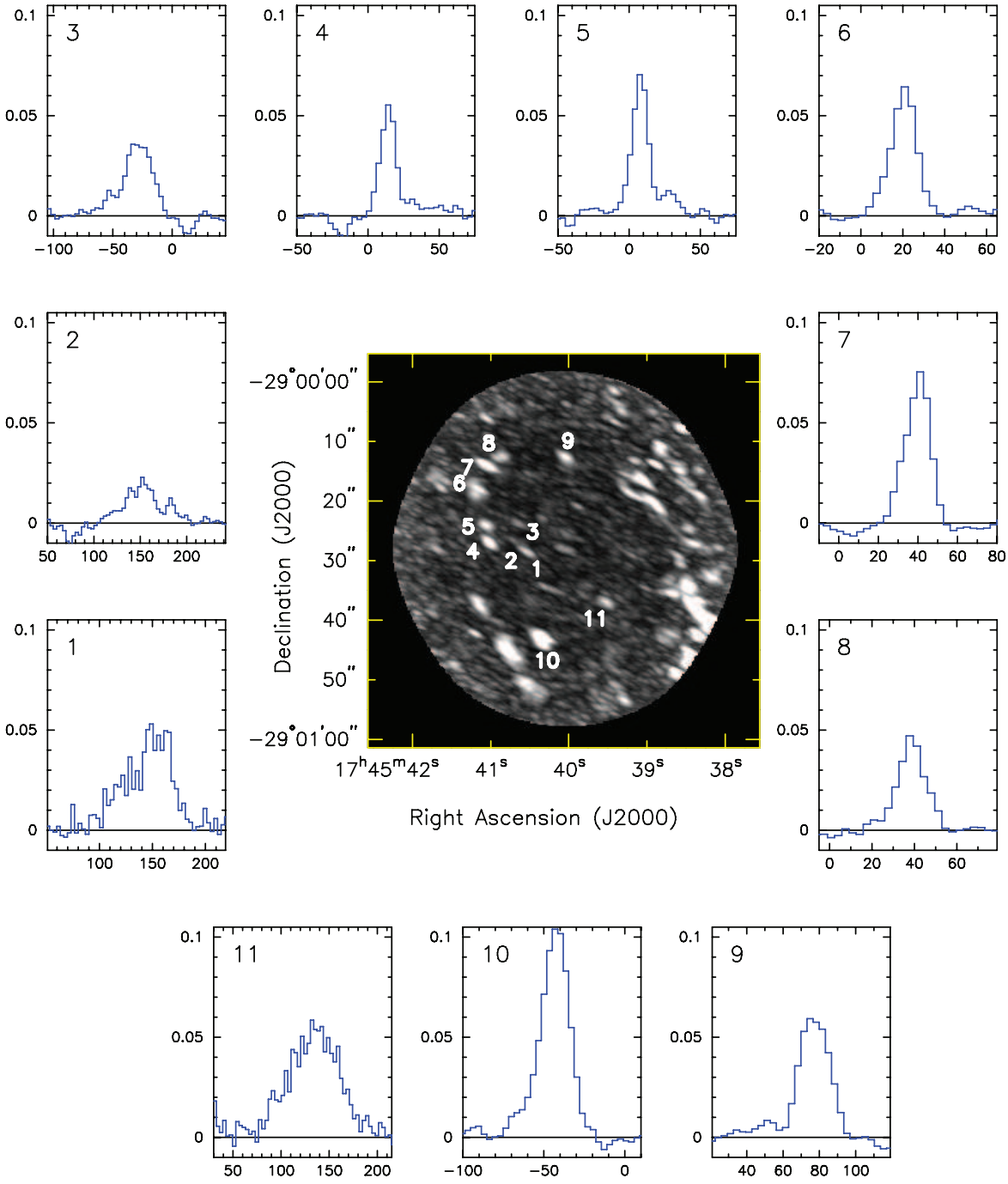

Fig. 2.— A grayscale image constructed from the peak SiO (5-4) line emission between $-191 < v < 213$ km s^{-1}. The inset shows the spectra of 11 SiO (5-4) clumps (mJy in Y-axis vs km s^{-1} in X-axis) within the molecular ring. The positions of labeled spectra are listed in Table 1.

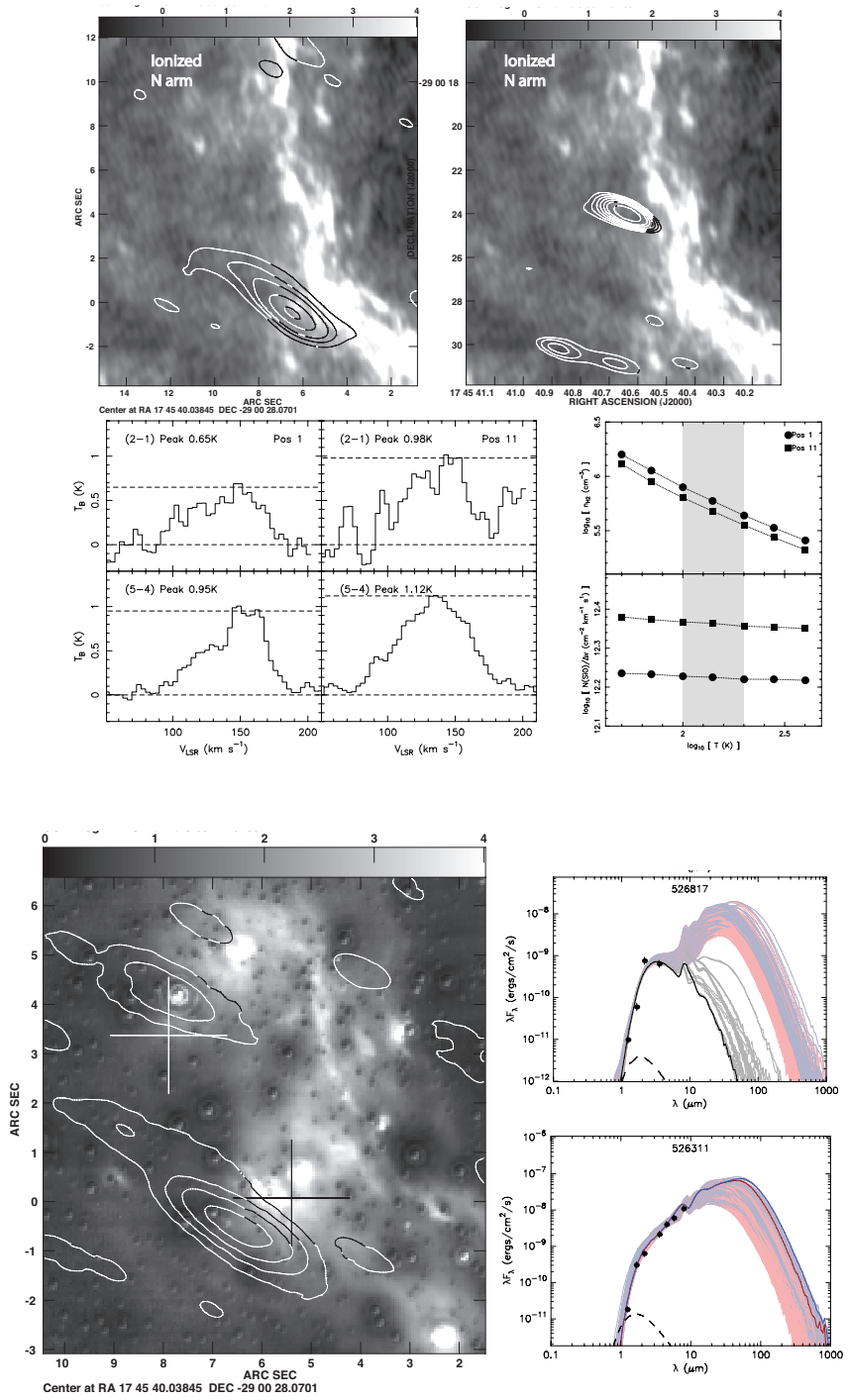

Fig. 3.— (a) Contours of SiO (5-4) line emission from Clumps 1 and 2 integrated between 88 and 188 km s^{-1} superimposed on a 3cm continuum image. (b) Same as (a) expect contours of SiO (5-4) line emission integrated over 0 and -50 km s^{-1} (c) the SiO (5-4) and (2-1) line profiles of Clumps 1 and 11. (d) The inferred H_2 density (Top) and the column density of SiO per linewidth (bottom) as a function of temperature. The band (grays) shows the temperature range of the CNR. (e) Contours of SiO(5-4) emission from Clumps 1 and 3 superimposed on ratio map of L (3.6μm) to K (1.6 μm) bands. The crosses show the positions of YSO candidates. (f) Fitted SEDs of the two YSO candidates 526311 and 526817 in the vicinity of Clumps 1 and 3, respectively.

Table 1. Gaussian Line Parameters of Fitted SiO Sources

Source	RA (J2000)	DEC (J200)	Peak mJy/beam	Center km s^{-1}	FWHM km s^{-1}	FWZI km s^{-1}
1	17:45:40.51	-29.0.28.78	38.91 ± 2.28	147.81 ± 1.35	47.42 ± 3.29	110 ± 40
2	17:45:40.74	-29.0.26.11	13.92 ± 1.36	159.81 ± 2.60	54.81 ± 6.39	120 ± 41
3	17:45:40.61	-29.0.23.90	35.43 ± 1.84	-27.86 ± 0.69	27.11 ± 1.66	55 ± 19
4	17:45:41.01	-29.0.27.03	77.75 ± 3.17	7.98 ± 0.23	11.52 ± 0.55	25 ± 9
5	17:45:41.06	-29.0.24.09	62.14 ± 3.19	14.28 ± 0.28	11.15 ± 0.66	18 ± 9
6	17:45:41.17	-29.0.17.84	67.20 ± 3.64	20.85 ± 0.34	12.92 ± 0.81	29 ± 10
7	17:45:41.03	-29.0.14.25	75.74 ± 2.80	38.98 ± 0.26	14.66 ± 0.63	31 ± 12
8	17:45:40.83	-29.0.12.78	48.81 ± 2.80	39.96 ± 0.44	15.65 ± 1.05	31 ± 13
9	17:45:40.03	-29.0.12.87	62.31 ± 2.53	77.80 ± 0.38	19.44 ± 0.93	40 ± 17
10	17:45:40.31	-29.0.43.77	71.32 ± 2.75	-42.98 ± 0.39	21.02 ± 0.95	56 ± 18
11	17:45:39.51	-29.0.36.96	50.43 ± 1.81	136.16 ± 0.96	55.51 ± 2.43	147 ± 39

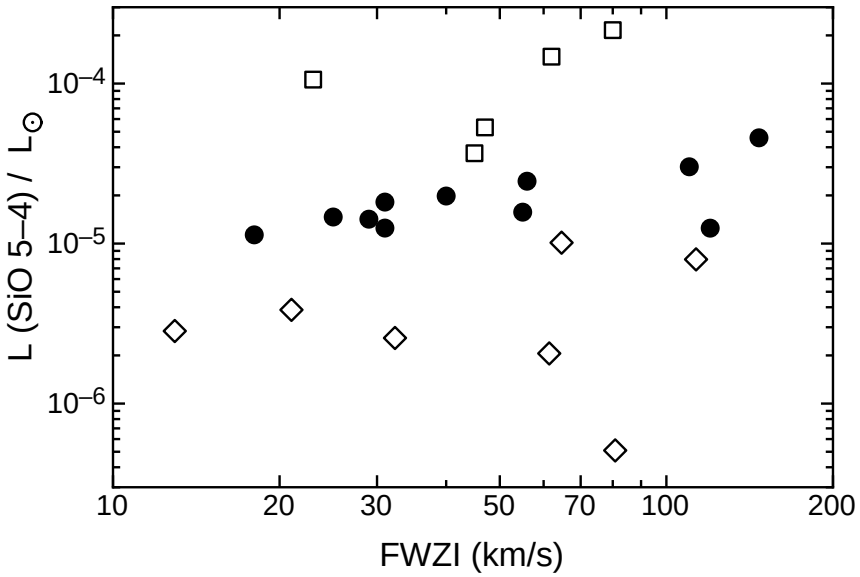

Fig. 4.— Filled circles show the luminosity in the SiO(5-4) line versus full line width (ie full width at zero intensity, FWZI) for the 11 sources detected in the circumnuclear ring. Open squares and open diamonds show the corresponding quantities for outflows from low-mass YSOs (Gibbs *et al.* 2004) and high-mass YSOs (Gibbs *et al.* 2007).